Multiobjective muffler shape optimization with hybrid acoustics modelling

Tuomas Airaksinen* Erkki Heikkola†

Abstract

Shape optimization of a duct system with respect to sound transmission loss is considered. The objective of optimization is to maximize the sound transmission loss at multiple frequency ranges simultaneously by adjusting the shape of a reactive muffler component. The noise reduction problem is formulated as a multiobjective optimization problem. The sound attenuation for each considered frequency is determined by a hybrid method, which requires solving Helmholtz equation numerically by finite element method. The optimization is performed using non-dominated sorting genetic algorithm, NSGA-II, which is a multi-objective genetic algorithm. The hybrid numerical method is flexible with respect to geometric shapes, material parameters and boundary conditions. Its combination with multiobjective optimization provides an efficient method to design muffler components.

1 Introduction

Physical phenomena encompass many forms of wave propagation and thus bring a great interest to understand wave propagation and its interaction with the environment. Acoustical applications reside in many disciplines, and often the goal is to reduce undesired acoustic noise. Sound propagation especially in waveguides is a fundamentally interesting topic. Ventilation ducts are an example of waveguide where noise reduction is of a special interest.

There are several methods to reduce noise in ducts. The noise reduction is achieved by mufflers, that are of either passive or active type. Passive mufflers fall into two categories: dissipative and reactive. Dissipative mufflers employ noise absorbing material and they are best suited for high frequency noise. Reactive mufflers exploit the shape of muffler component to obtain useful wave reflections and they are best suited at low frequencies. Active mufflers, for one, implement noise reduction by creating antinoise of the same amplitude but opposite phase to the original noise,

*Department of Mathematical Information Technology, University of Jyväskylä, PO Box 35 (Agora), FI-40014 University of Jyväskylä, Finland, tuomas.airaksinen@jyu.fi

†Numerola Oy, P.O. Box 126, FI-40101 Jyväskylä, Finland erkki.heikkola@numerola.fi

see for example Egena et al.[1] and Lee et al[2]. They are effective at low frequency noise cancellation.

The study of acoustical sound propagation in ducts is possible by several means. Experimental acoustical study is often not feasible, whereas analytical or numerical methods can often be considered. There is a introduction to one dimensional duct acoustic modeling in Munjal[3]. Four-pole transfer matrix method, that is based on plane wave theory, offers an approximative way to make a one-dimensional model of muffler acoustics. This approach has been used for transmission loss optimization in duct system in Yeh et al[4]. However, the method is limited to simple geometries and boundary conditions.

The finite element method (FEM) is a general approach to solve approximately partial differential equations. By FEM, it is possible to obtain approximate, yet accurate solution of Helmholtz equation with appropriate boundary conditions. It is also possible to consider problems with complex geometry and varying material properties. By using suitable preconditioner, such as one introduced in Airaksinen et al.[5], it is possible to solve effectively large Helmholtz problems.

In this article, the modelling of an acoustic reactive muffler is based on a hybrid numerical method[6]. This method provides realistic modelling of acoustics in a muffler component, which is located between uniform inlet and outlet ducts. In the uniform parts, acoustic solution can be obtained by modal analysis, where individual propagating modes are solved numerically or in special cases, analytically. For example in circular ducts, solution of the Helmholtz equation can be represented in terms of Bessel functions. Finite element method is used to solve the Helmholtz equation in the non-uniform muffler part of the ductwork. Mode matching[7] is used to couple the different solutions in the muffler and inlet/outlet ducts. The generality of finite element method is thus provided to the acoustics simulation and complicated shapes and configurations can be treated accurately.

The objective of optimization here is to maximize the sound transmission loss (STL) of the muffler by utilizing shape optimization at two frequency ranges simultaneously. In book by Haslinger and Mäkinen[8], an introduction to shape optimization has been given. In addition to shape optimization, material parameters, especially absorption of the boundary material could also be optimized by applying the method of this paper.

As an optimization method, a genetic algorithm (GA) is considered, which is a stochastic optimization algorithm that mimics genetic drift and the Darvinian strife for survival. Unlike traditional gradient-based optimizers that need the derivatives and a good starting point, GA has a good opportunity to locate the global optimum in a near optimal manner. In Mäkinen et al. [9], a genetic algorithm approach to multiobjective aircraft wing shape optimization has been proposed. Here, the optimization is made with the non-dominated sorting genetic algorithm, NSGA-II [10], which is an optimizer well suited for multi-objective problems.

The article is organized as follows. In Section 2, the mathematical formulation of the acoustics in the muffler component is given. Hybrid numerical method is described in Section 3. In Section 4, numerical experiments are performed and results

are reported. In Section 5, the concluding remarks are given.

2 Mathematical formulation

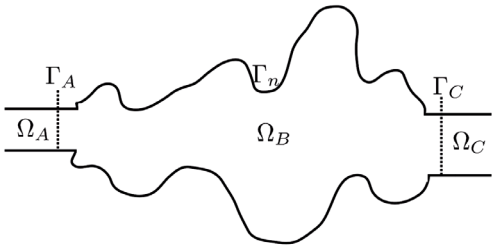

Figure 1: The crosscut illustration of a duct system in a general case: inlet pipe Ω_A, muffler component of arbitrary shape Ω_B and outlet pipe Ω_C.

Sound propagation is governed by the acoustic wave equation

$$c^2 \boldsymbol{\nabla} \cdot \frac{1}{\rho} \boldsymbol{\nabla} \tilde{p} - \frac{1}{\rho} \frac{\partial^2 \tilde{p}}{\partial t^2} \;=\; 0, \tag{1}$$

where $\tilde{p}\,(\mathbf{x}, t)$ is the pressure field at location $\mathbf{x}$ and time t, $\rho\,(\mathbf{x})$ is the density of the material, $c\,(\mathbf{x})$ is the speed of sound. Assuming time-harmonic pressure field $\tilde{p}\,(\mathbf{x}, t) = p\,(\mathbf{x})\; e^{-i\omega t}$, where ω is angular frequency and $i = \sqrt{-1}$, Eq. (1) leads to the Helmholtz equation

$$-\boldsymbol{\nabla} \cdot \frac{1}{\rho} \boldsymbol{\nabla} p - \frac{k^2}{\rho} p \;=\; 0, \tag{2}$$

where $k = \omega / c$ is the angular wavenumber.

The duct system is illustrated in Fig. 1. It consists of three parts: inlet duct domain Ω_A, muffler component domain Ω_B and outlet duct domain Ω_C. Inlet and outlet ducts must have uniform but arbitrary cross-section. Inlet and outlet ducts are connected to a general, arbitrarily shaped muffler component on interfaces Γ_A and Γ_C. The wall of the muffler is denoted by domain Γ_n, thus $\partial\Omega_B = \Gamma_A \cup \Gamma_n \cup \Gamma_C$. Non-absorbing sound-hard boundary is considered on Γ_n, and it is modelled by Neumann boundary condition

$$\mathbf{n} \cdot \boldsymbol{\nabla} p \;=\; 0 \quad \text{on } \Gamma_n, \tag{3}$$

where $\mathbf{n}$ is the outer normal vector on boundary Γ_n.

The solution of Helmholtz equation Eq. (2) in muffler component domain Ω_B is obtained by finite element method, which is described later in Section 3. In duct domains Ω_A and Ω_C, Helmholtz solution can be obtained by modal analysis. In certain special cases such as circular or rectangular duct, analytical form of the solution

can be derived, whereas in general shaped duct, eigenfunctions have to be solved numerically. The expansion of the acoustic pressure in duct domains Ω_A and Ω_C is represented in cylindrical coordinates as a sum over the eigenmodes

$$\begin{aligned} p_A(r,\theta,z) &= \sum_{j=0}^{m_A} A_j \Phi_j(r,\theta)\, e^{-i\lambda_j z} + \sum_{j=0}^{m_A} F_j \Phi_j(r,\theta)\, e^{i\lambda_j z} \qquad \text{and} \\ p_C(r,\theta,z) &= \sum_{j=0}^{m_C} B_j \Psi_j(r,\theta)\, e^{-i\gamma_j z} + \sum_{j=0}^{m_C} C_j \Psi_j(r,\theta)\, e^{i\gamma_j z}, \end{aligned} \tag{4}$$

where $\Phi_j(r,\theta)$ and $\Psi_j(r,\theta)$ are transverse duct eigenfunctions corresponding to the cross-section of the pipe, F_j, A_j, B_j and C_j are the modal amplitudes corresponding to eigenfunctions Ψ_j, Φ_j, and λ_j, γ_j are axial wavenumbers along z-axis. As the evanescent modes can be truncated, sums in Eq. (4) have only finite number propagating modes, denoted by m_A, m_C. Coordinate systems in uniform ducts are chosen such that z-coordinate gives the axial direction of the duct with positive direction away from the nonuniform domain Ω_B. The origin of coordinate system in domain Ω_A is located on the interface Γ_A, and the origin of Ω_C is located on Γ_C.

Coefficients F_j determine the incoming sound from inlet pipe. The equal modal energy density (EMED) assumption, i.e. $|F_n|^2 I_n = |F_m|^2 I_m$ for all m, n, has been chosen for the inlet as incident sound source, as it is a good representation of the sound field emanating from a fan in a ventilation system; see Kirby and Lawrie[11]. For EMED, the incoming modal amplitudes can be calculated from the formula

$$|F_n|^2 = \frac{I_0}{I_n \sum_{m=0}^{n_F} \lambda_m}. \tag{5}$$

Modal amplitude coefficients A_j correspond to the sound that is reflected back from the muffler, B_j correspond to the sound propagating to the outlet pipe and C_j correspond to the sound that is reflected back from outlet pipe. By setting $C_j = 0$ for all j, a perfectly non-reflecting boundary is imposed on Γ_C.

The sound transmission loss function is defined as the ratio of the transmitted to incident sound powers

$$TL(\mathbf{x},f) = -10\,\log_{10} \frac{\rho_A \sum_{m=0}^{n_B} \gamma_m H_m |B_m|^2}{\rho_C \sum_{m=0}^{n_B} \lambda_m I_m |F_m|^2}, \tag{6}$$

where $I_n = \int_{\Gamma_A} |\Phi_n|^2\, dx$ and $H_m = \int_{\Gamma_B} |\Psi_m|^2\, dx$. By considering the EMED assumption Eq. (5), we can write the ratio the transmission loss in a simpler form

$$TL(\mathbf{x},f) = -10\,\log_{10} \frac{\rho_A \sum_{m=0}^{n_B} \gamma_m H_m |B_m|^2}{\rho_C I_0}. \tag{7}$$

Next, function $\tau(\mathbf{x},f)$ is defined as

$$\tau(\mathbf{x},f) = \min\left(TL(\mathbf{x},f), TL_{max}\right). \tag{8}$$

Here, parameter TL_{max} is a limiting value for transmission loss, which is necessary due to possible narrow infinite peaks in transmission loss function that inhibit good convergence of the optimizer.

The multiobjective optimization problem is defined as a minimization of objective functions

$$f_1(\mathbf{x}) = -\frac{1}{n_1}\sum_{i=1}^{n_\omega}\tau(\mathbf{x},\omega_i) \qquad \text{and} \qquad f_2(\mathbf{x}) = -\frac{1}{n_2}\sum_{i=1}^{n_\iota}\tau(\mathbf{x},\iota_i), \tag{9}$$

where the shape vector $\mathbf{x} = [x_1, \ldots, x_{n_{vars}}]$ contains parameters that are used to alter the shape of the muffler component, $\boldsymbol{\omega} = [\omega_1, \ldots, \omega_{n_\omega}]$ and $\boldsymbol{\iota} = [\iota_1, \ldots, \iota_{n_\iota}]$ are vectors of frequencies where sound transmission loss is maximized.

2.1 Eigenfunctions in a circular duct

In circular duct, the eigenfunctions $\Phi_j(r,\theta)$ and $\Psi_j(r,\theta)$ are represented by modes

$$\Phi_j(r,\theta) \;=\; J_{m_j}(k_{rj}r)\,e^{im_j\theta}, \tag{10}$$

where $J_{m_j}(x)$ is order m_j Bessel function of the first kind and k_{rj} is the radial wavenumber. The radial wavenumber k_{rj} is obtained by considering sound-hard wall boundary condition $\mathbf{n}\cdot\boldsymbol{\nabla}p = 0$, which here implicates that at $r = a$, where a is the radius of the duct wall,

$$J'_{m_j}(k_{rj}a) \;=\; 0. \tag{11}$$

Axial wavenumber k_{zj} is evaluated from the effective wavenumber k and the radial wavenumber k_{rj} by

$$k_{zj} \;=\; \sqrt{k^2 - k_{rj}^2}. \tag{12}$$

The axial wave propagation is determined by term $e^{ik_{zj}z}$ (see Eq. (4)), which implicates that imaginary axial wavenumber k_{zj} leads to exponential decaying of the wave mode. Thus, the evanescent modes with $k_{rj} > k$ are neglected. Modes are denoted by index j that starts from zero and is ordered according to the radial wavenumbers k_{rj}. The radial wavenumbers are calculated from Bessel derivative roots $k_{rj} = b_j/a$ according to Eq. (11) (see Table 1), where b_j is the root of Bessel derivate of order m_j and a is the radius of the duct.

Table 1: First roots of Bessel derivative function, $J'_{m_j}(b_j) = 0$.

j	1	2	3	4	5
m_j	0	1	2	0	3
b_j	0.0	1.84	3.05	3.83	4.20

3 Hybrid numerical method with mode matching

In the hybrid numerical method, the modal representations in Ω_A and Ω_C are coupled to the finite element representation in Ω_B by mode matching. The weak formulation of the Helmholtz equation Eq. (2) is the following: find $p_B = p_r + p_i i$, where $p_r \in H^1(\Omega_B)$, $p_i \in H^1(\Omega_B)$, such that

$$\int_{\Omega_B} \frac{1}{\rho} \left(\boldsymbol{\nabla} p_B \cdot \boldsymbol{\nabla} v - k^2 p_B v \right) dx - \int_{\partial\Omega_B} \frac{1}{\rho} \mathbf{n} \cdot \boldsymbol{\nabla} p_B \, v \, dx = 0 \tag{13}$$

for any $v \in H^1(\Omega_B)$; $\mathbf{n}$ is outward normal vector. Solution p_A and p_C are coupled to p_B by the boundary conditions

$$\mathbf{n} \cdot \nabla p_B = \mathbf{n} \cdot \nabla p_A \quad \text{on } \Gamma_A, \tag{14}$$
$$\mathbf{n} \cdot \nabla p_B = \mathbf{n} \cdot \nabla p_C \quad \text{on } \Gamma_C, \tag{15}$$
$$p_B = p_A \quad \text{on } \Gamma_A, \tag{16}$$
$$p_B = p_C \quad \text{on } \Gamma_C. \tag{17}$$

The first two conditions Eqs. (14) and (15) and Neumann condition Eq. (3) can be incorporated in the weak form Eq. (13), leading to the equation

$$\int_{\Omega_B} \frac{1}{\rho} \left(\boldsymbol{\nabla} p_B \cdot \boldsymbol{\nabla} v - k^2 p_B v \right) dx - \int_{\Gamma_A} \frac{1}{\rho} \mathbf{n} \cdot \boldsymbol{\nabla} p_A \, v \, dx - \int_{\Gamma_C} \frac{1}{\rho} \mathbf{n} \cdot \boldsymbol{\nabla} p_C \, v \, dx = 0. \tag{18}$$

In mode matching, the two other conditions Eqs. (16) and (17) are imposed in weak forms: find $p_A \in Z_A$, $p_B = p_r + p_i i$, where $p_r \in H^1(\Omega_B)$, $p_i \in H^1(\Omega_B)$ and $p_C \in Z_C$ such that

$$\begin{aligned} \int_{\Gamma_A} (p_B - p_A) \, \bar{\Phi}_i dx &= 0 \text{ and} \\ \int_{\Gamma_C} (p_B - p_C) \, \bar{\Psi}_i dx &= 0 \end{aligned} \tag{19}$$

for any $\bar{\Phi}_i \in Z_A$ and $\bar{\Psi}_i \in Z_C$, where test function spaces are defined as $Z_A = \text{span}_{j=0,\ldots,m_A} \{\Phi_j(r,\theta)\}$ and $Z_C = \text{span}_{j=0,\ldots,m_C} \{\Psi_j(r,\theta)\}$. In summary, the hybrid formulation of the acoustic problem in the waveguide is given by the Eqs. (18) and (19).

Finite element discretization proceeds by approximating the acoustic pressure in Ω_B by

$$p_B(x) = \sum_{j=1}^{n} N_j(x) \, p_j = [N_1(x), \ldots, N_n(x)] \begin{bmatrix} p_1 \\ \vdots \\ p_n \end{bmatrix} = \mathbf{N}(x)^T \mathbf{p}, \tag{20}$$

where $N_j(x)$ are global trial functions for finite element mesh, p_j are the nodal values of the acoustic pressure at node j and n is the number of nodes in Ω_B. Galerkin method of weighted residuals proposes that $N_j(x)$ are used as test functions v. The approximation Eq. (20) is next replaced in Eq. (18) to form a matrix equation

$$\int_{\Omega_B} \frac{1}{\rho} \left(\boldsymbol{\nabla}\mathbf{N} \cdot \boldsymbol{\nabla}\mathbf{N}^T - k^2 \mathbf{N}\mathbf{N}^T \right) dx\, \mathbf{p} - \int_{\Gamma_A} \frac{1}{\rho} \mathbf{N}\, \mathbf{n} \cdot \boldsymbol{\nabla} p_A\, dx - \int_{\Gamma_C} \frac{1}{\rho} \mathbf{N}\, \mathbf{n} \cdot \boldsymbol{\nabla} p_C\, dx = 0 \quad (21)$$

The modal representations of the solutions p_A and p_C in Eq. (4) are replaced into Eq. (21), where the normal derivatives of p_A and p_C are of the form

$$\begin{aligned} \mathbf{n} \cdot \boldsymbol{\nabla} p_A(r,\theta,0) = \frac{\partial}{\partial z} p_A(r,\theta,0) &= -i \sum_{j=0}^{m_A} \lambda_j A_j \Phi_j + i \sum_{j=0}^{m_A} \lambda_j F_j \Phi_j, \\ \mathbf{n} \cdot \boldsymbol{\nabla} p_C(r,\theta,0) = \frac{\partial}{\partial z} p_C(r,\theta,0) &= -i \sum_{j=0}^{m_C} \gamma_j B_j \Psi_j. \end{aligned} \quad (22)$$

These derivatives are substituted in Eq. (21):

$$\begin{aligned} \int_{\Omega_B} \frac{1}{\rho} \left(\boldsymbol{\nabla}\mathbf{N} \cdot \boldsymbol{\nabla}\mathbf{N}^T - k^2 \mathbf{N}\mathbf{N}^T \right) dx\, \mathbf{p} - \int_{\Gamma_A} \frac{1}{\rho} \mathbf{N} \left(-i \sum_{j=0}^{m_A} \lambda_j A_j \Phi_j + i \sum_{j=0}^{m_A} \lambda_j F_j \Phi_j \right) dx \\ - \int_{\Gamma_C} \frac{1}{\rho} \mathbf{N} \left(-i \sum_{j=0}^{m_C} \gamma_j B_j \Psi_j \right) dx = 0. \end{aligned} \quad (23)$$

This is expanded in component form

$$\begin{aligned} \sum_{j=0}^{n_A} \int_{\Omega_B} \frac{1}{\rho} \left(\boldsymbol{\nabla} N_i \cdot \boldsymbol{\nabla} N_j - k^2 N_i N_j \right) dx\, p_j + i \sum_{j=0}^{m_A} \lambda_j \int_{\Gamma_A} \frac{1}{\rho} N_i \Phi_j\, dx\, A_j \\ - i \sum_{j=0}^{m_A} \lambda_j \int_{\Gamma_A} \frac{1}{\rho} N_i \Phi_j\, dx\, F_j + i \sum_{j=0}^{m_C} \gamma_j \int_{\Gamma_C} \frac{1}{\rho} N_i \Psi_j\, dx\, B_j = 0. \end{aligned} \quad (24)$$

If we use the matrix notations

$$\begin{array}{llll} \hat{H}_{ij} = i\lambda_j \int_{\Gamma_A} \frac{1}{\rho} N_i \Phi_j\, dx & & \hat{K}_{ij} = i\gamma_j \int_{\Gamma_C} \frac{1}{\rho} N_i \Psi_j\, dx & \\ \tilde{f}_i = i \sum_{j=0}^{m_A} \lambda_j \int_{\Gamma_A} \frac{1}{\rho} N_i \Phi_j\, dx\, F_j & & G_{ij} = \int_{\Omega_B} \frac{1}{\rho} \left(\boldsymbol{\nabla} N_i \cdot \boldsymbol{\nabla} N_j - k^2 N_i N_j \right) dx, & \end{array} \quad (25)$$

we can write (24) in matrix form

$$\hat{\mathbf{H}}\mathbf{a} + \mathbf{G}\mathbf{p} \quad + \hat{\mathbf{K}}\mathbf{b} = \quad \tilde{\mathbf{f}}, \quad (26)$$

where $\mathbf{a}$ contains m_A complex modal amplitudes of interface Γ_A, $\mathbf{b}$ contains m_B complex modal amplitudes of interface Γ_B.

Eqs. (4) and (20) are next replaced in Eq. (19):

$$\begin{aligned}\int_{\Gamma_A} \bar{\Phi}_i \mathbf{N}^T \, dx \, \mathbf{p} &= \sum_{j=0}^{m_A} \int_{\Gamma_A} \Phi_j \bar{\Phi}_i \, dx \, A_j + \sum_{j=0}^{m_A} \int_{\Gamma_A} \Phi_j \bar{\Phi}_i \, dx \, F_j, \\ \int_{\Gamma_B} \bar{\Psi}_i \mathbf{N}^T \, dx \, \mathbf{p} &= \sum_{j=0}^{m_C} \int_{\Gamma_A} \Psi_j \bar{\Psi}_i \, dx \, B_j. \end{aligned} \tag{27}$$

Expanded to components, this reads

$$\begin{aligned}\sum_{j=0}^{n} \int_{\Gamma_A} \bar{\Phi}_i N_j \, dx \, p_j &= \sum_{j=0}^{m_A} \int_{\Gamma_A} \Phi_j \bar{\Phi}_i \, dx \, A_j + \sum_{j=0}^{m_A} \int_{\Gamma_A} \Phi_j \bar{\Phi}_i \, dx \, F_j, \\ \sum_{j=0}^{n} \int_{\Gamma_B} \bar{\Psi}_i N_j \, dx \, p_j &= \sum_{j=0}^{m_C} \int_{\Gamma_A} \Psi_j \bar{\Psi}_i \, dx \, B_j. \end{aligned} \tag{28}$$

By using matrix notations

$$\begin{aligned} H_{ij} &= \textstyle\int_{\Gamma_A} \Phi_j \bar{\Phi}_i \, dx & \qquad K_{ij} &= \textstyle\int_{\Gamma_C} \Psi_j \bar{\Psi}_i \, dx \\ \tilde{H}_{ij} &= -\textstyle\int_{\Gamma_A} \bar{\Phi}_i N_j \, dx & \qquad \tilde{K}_{ij} &= -\textstyle\int_{\Gamma_C} \bar{\Psi}_i N_j \, dx \\ f_i &= -\textstyle\sum_{j=0}^{m_A} \int_{\Gamma_A} \Phi_j \bar{\Phi}_i \, dx \, F_i, \end{aligned} \tag{29}$$

Eq. (28) can be written in matrix form

$$\begin{aligned} \mathbf{H}\mathbf{a} + \tilde{\mathbf{H}}\mathbf{p} &= \mathbf{f} \\ \mathbf{K}\mathbf{b} + \tilde{\mathbf{K}}\mathbf{p} &= \mathbf{0}. \end{aligned} \tag{30}$$

Now, the Eqs. (26) and (30) can be written as a single block matrix equation

$$\begin{bmatrix} \mathbf{H} & \tilde{\mathbf{H}} & 0 \\ \hat{\mathbf{H}} & \mathbf{G} & \hat{\mathbf{K}} \\ 0 & \tilde{\mathbf{K}} & \mathbf{K} \end{bmatrix} \begin{bmatrix} \mathbf{a} \\ \mathbf{p} \\ \mathbf{b} \end{bmatrix} = \begin{bmatrix} \mathbf{f} \\ \tilde{\mathbf{f}} \\ 0 \end{bmatrix}. \tag{31}$$

4 Numerical experiments

In this section, the multiobjective minimization of the functions f_1 and f_2 in Eq. (9) is tested in four different cases. In each case, the shape of the muffler is controlled with certain shape parameters $\mathbf{x}$ and the goal is to improve attenuation at given frequencies. The test problem #1 represents a non-symmetric three-dimensional muffler component optimization. The test problem #2 is chosen because similar optimization has been considered in Barbieri and Barbieri [12]. The test problem #3 has been chosen as an example of a problem that has many parameters defining the shape. The last test problem #4 is Helmholtz resonator that has been considered in Selamet et al[13]. It has been chosen as second example that represents non-symmetric three-dimensional geometry.

4.1 Technical details

The non-dominated sorting genetic algorithm[10] (NSGA-II) is used as a generic multi-objective optimizer. It is chosen as an optimizer due to local minima and non-linear nature of the problem. The following parameters are used in genetic algorithm. The population size $n_{pop} = 50$ is used in examples #1 and #2 and $n_{pop} = 100$ in examples #3 and #4. At the beginning of optimization, a random population of size $10\, n_{pop}$ is generated, and then the best candidates are chosen to initial population. The crossover probability is set to $p_c = 0.9$. The mutation probability is set to $p_m = 1/n_{vars}$, where n_{vars} is the number of optimization variables in the problem. Binary selection is used and simulated binary crossover (SBX) operator and polynomial mutation operator [14] are utilized with distribution indices $\eta_c = 20$, $\eta_m = 10$, respectively.

The three-dimensional tetrahedral meshes for test problems are generated by freely available Netgen mesh generator[15] and the finite element approximation of the pressure field in muffler component is evaluated by a code written in Numerrin language[16], which is a modelling language developed by Numerola Ltd. Quadratic tetrahedral elements are used in order to reduce the error from approximation of rounded surfaces and finite element pollution effect [17]. The shape of the muffler component is altered with respect to chosen variables in order to obtain optimal transmission loss for the muffler component at chosen frequency ranges. The problem is formulated as a multiobjective optimization problem, as described in Section 2. In numerical experiments, meshes are generated such that there are at least ten elements per wave length at the highest considered frequency. The number of elements in test problems are around 2000. The limiting value $TL_{max} = 50$ dB (see Eq. (8)) is used in all examples.

4.2 Test problem #1

The dimensions and a schematic illustration of the muffler component are presented in Fig. 2a. The length of the chamber is $L = 500$ mm. The radius of inlet and outlet ducts are $r = 30$ mm. The problem has three variables that are optimized: the location of inlet duct $x_1 \in [0.1, 0.5]$, the location of outlet duct $x_2 \in [0.25, 0.5]$ and the radius of muffler chamber $x_3 = [0.04, 0.08]$. Transmission loss is optimized in frequency ranges 800-900 Hz and 1700-1800 Hz. Two sets of frequencies are optimized according to the formulation in Eq. (9): $\boldsymbol{\omega} = [800, 825, 850, 875, 900]$ Hz and $\boldsymbol{\iota} = [1700, 1725, 1750, 1775, 1800]$ Hz. The objective function values in initial population are on average $f_1 = -14.6$ dB and $f_2 = -11.7$ dB.

In Fig. 2b, there are four non-dominated fronts (approximations of pareto optimal fronts) that are obtained by NSGA-II algorithm after 100 generations. The different fronts in the figure are obtained by using different random number generator seed numbers. It is seen, that different fronts are mostly converged to the same line. This implicates that the algorithm is behaving robustly. It is also seen that after optimization, the objectives are over 20 dB better than before optimization.

In Fig. 3b, the transmission loss as a function of frequency is plotted for an optimal solution that is chosen from the non-dominated front at point $f_1 = -38.3$ dB , $f_2 = -33.4$ dB which is given by shape parameter vector $\mathbf{x} = [0.16, 0.37, 0.08]$. It is seen that the transmission loss is significantly greater at optimized frequency ranges than elsewhere.

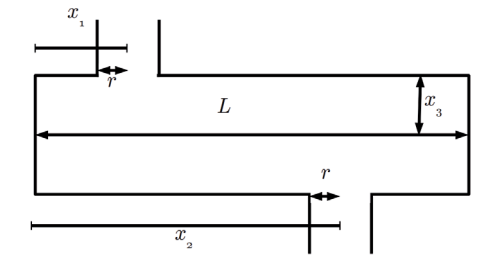

(a)

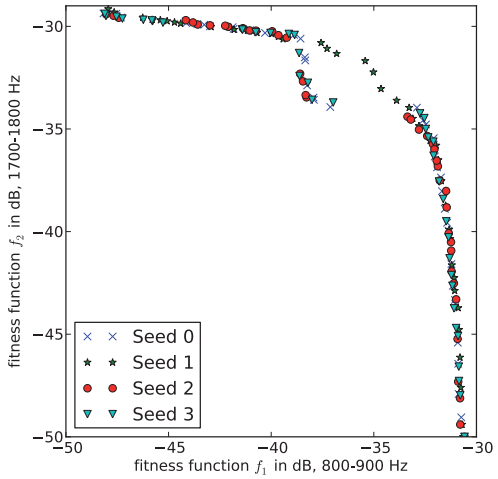

(b)

Figure 2: In the upper figure, there is a diagram of a muffler component cross section used in test case #1. In the lower figure, there are non-dominated solution fronts for test case #1, four different random seeds.

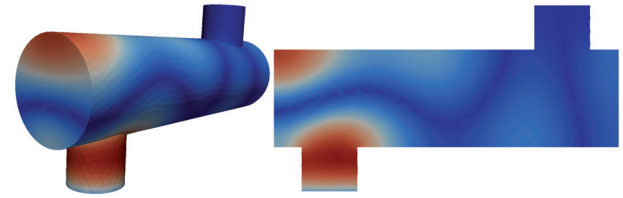

(a)

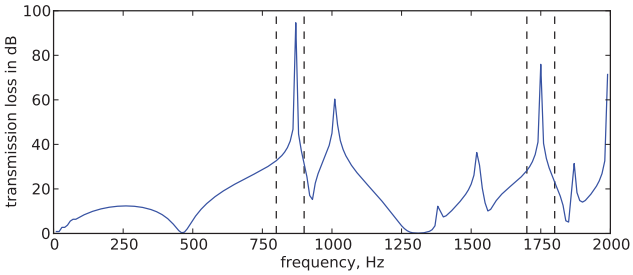

(b)

Figure 3: In the upper figures, there is the time average of pressure for optimal solution of test problem #1. The frequency is $f = 1800$ Hz and optimized parameters are $\mathbf{x} = [0.16, 0.37, 0.08]$ mm. The solution is chosen from non-dominated front at point $f_1 = -38.3$ dB , $f_2 = -33.4$ dB. In the lower figure there is the transmission loss as a function of frequency. Transmission loss is maximized in frequency ranges 800-900 Hz and 1700-1800 Hz.

4.3 Test problem #2

The second numerical example problem is illustrated in Fig. 4a. The geometry of the problem is the same as in Barbieri and Barbieri[12]. The diameter of the chamber is $D = 153.2$ mm and the length of the chamber $L = 282.3$ mm. Inlet and outlet duct diameters are $d = 48.6$ mm. The problem has two variables to be optimized: lengths of the inlet and outlet ducts inside the muffler chamber $x_1, x_2 \in [10, 250]$ mm, respectively.

In Barbieri and Barbieri[12], the tests were reduced to two dimensional domains using axisymmetry, whereas our similations are performed in three-dimensional domains. As an optimizer, the Zoutendijk's feasible direction method was used in Barbieri and Barbieri[12], whereas NSGA-II is considered here. The NSGA-II method brings two obvious advantages: the problem may be formulated as a multi-objective optimization problem and there is no need to choose a good starting point for the algorithm.

Transmission loss is optimized around frequency ranges 600-650 Hz and 1200-1250 Hz. Two sets of frequencies used in Eq. (9) are $\boldsymbol{\omega} = [600, 625, 650]$ Hz and $\boldsymbol{\iota} = [1200, 1225, 1250]$ Hz. The objective function values in initial population are on average $f_1 = f_2 = -10$ dB.

The Fig. 5 shows the non-dominated fronts of objective functions in Eq. (9) given by NSGA-II after 50 generations for the problem when using four different seed number for random number generator. It is seen that fronts have converged to same line and that significant improvement in transmission loss values have been gained at both frequency ranges. It is obvious that the best compromise of the optimal value is found at the edge at point $f_1 = -32.0$ dB, ,$f_2 = -35.4$ dB in Fig. 5. The optimal solution is obtained with parameters $x_1 = 125$ mm and $x_2 = 58$ mm. In Fig. 6, the transmission loss as a function of frequency is plotted. It is seen, that at optimized frequency ranges, there are improvement in transmission loss.

The results obtained in Barbieri and Barbieri[12] (Example 2 in Section 4.2) are very similar to the results obtained here. The optimization method finds a solution where a transmission loss peak in both optimized frequency ranges occur. The method described here is more general and easily used in general three-dimensional problems.

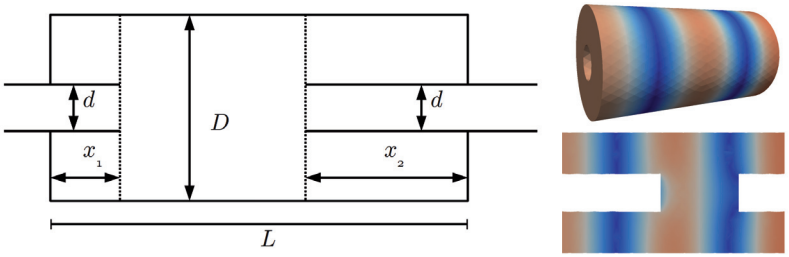

(a) (b)

Figure 4: On the left figure, there is the diagram of a muffler component used in test case #2. On the right figure, the time average of pressure for optimal solution is plotted. The frequency is $f = 1225$ Hz and optimized parameters are $x_1 = 125.2$ mm, $x_2 = 58.1$ mm. The solution is chosen from non-dominated front at $f_1 = -32.0\,, f_2 = -35.4$.

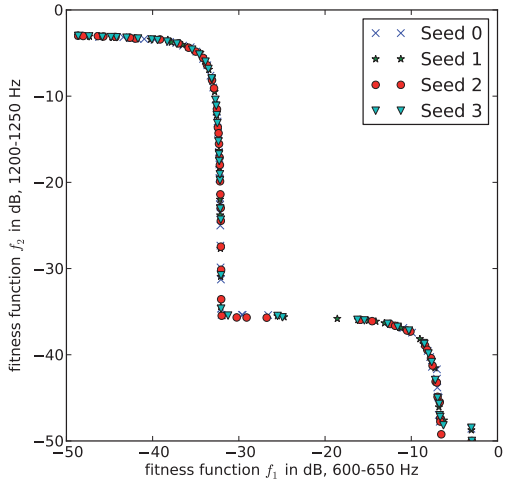

Figure 5: The non-dominated fronts for test case #2, four different random seeds.

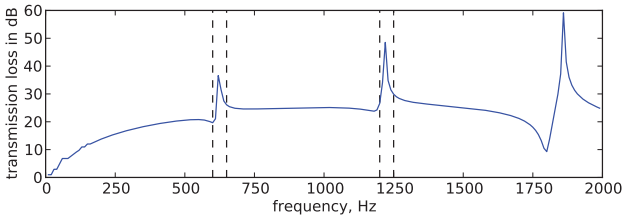

Figure 6: The transmission loss as a function of frequency is plotted. Transmission loss is maximized in frequency ranges 600-650 Hz and 1200-1250 Hz. The optimal parameters $x_1 = 125.2$ mm, $x_2 = 58.1$ mm that are chosen from non-dominated front at $f_1 = -32.0$ dB, $f_2 = -35.4$ dB are used.

4.4 Test problem #3

As an example of a problem that has more optimization variables, a muffler component that consists of five cylinders with variable radii is considered. In Fig. 7a, a schematic figure of the problem is presented. In addition to the radius of each cylinder, the length of inlet and outlet ducts are variable as well, similarly to the test problem #2. The length of muffler component is $L = 1000$ mm and the diameters of inlet and outlet ducts are $d = 100$ mm. The length of inlet and outlet ducts x_1, x_2 can vary between $[20, 900]$ mm and the diameter of each cylinder $x_{3...7}$ is between $[120, 240]$ mm. Transmission loss is optimized in two frequency ranges: between 200-300 Hz and 500-600 Hz, and the frequency sets (see Eq. (9)) are set to $\boldsymbol{\omega} = [200, 233, 266, 300]$ Hz and $\boldsymbol{\iota} = [500, 533, 566, 600]$ Hz. The population size was set to $n_{pop} = 100$ due to larger number of optimization variables.

In Fig. (8), there are four non-dominated fronts of objective functions in Eq. (9) that are obtained by NSGA-II after 120 generations. Also here it is seen that fronts are converged to the same line. Before optimization, the average values of the fitness function values of randomly generated initial population were $f_1 = -13$ dB and $f_2 = -15$ dB.

In Fig. 9, the transmission loss as a function of frequency is plotted for an optimal solution that is chosen from the non-dominated front at $f_1 = -43.16$ dB, $f_2 = -42.97$ dB. The optimal parameters for the chosen solution are $\mathbf{x} = [35.6, 35.3, 21.0, 24.0, 12.0, 24.0, 14.8]$ mm. The same parameters are used also when plotting the example solution in Fig. 7b. It is seen in Fig. 9 that both frequency ranges significantly improved transmission loss level.

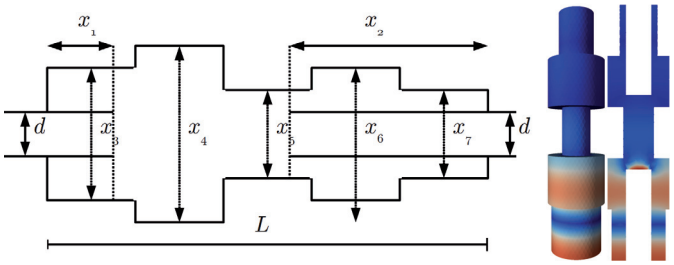

(a) (b)

Figure 7: On the left figure, there is a diagram of a muffler component used in test case #3. On the right figure, the pressure time average of optimal solution is plotted for test case #3 at $f = 600$ Hz. The figure is rotated 90°, such that inlet appears on the bottom of the figure.

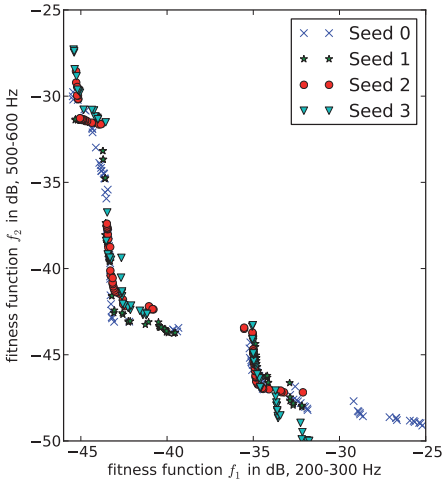

Figure 8: The non-dominated fronts for test case #3 are plotted, four different random seeds.

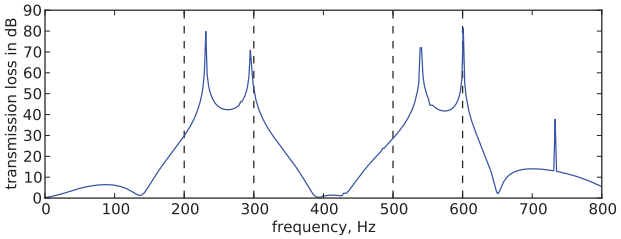

Figure 9: The transmission loss as a function of frequency. Transmission loss is maximized at frequency ranges 200-300 Hz and 500-600 Hz.

4.5 Test problem #4

Fourth example is a Helmholtz resonator component similar to the example used in Selamet et al.[13], that represents an example of true three-dimensional geometry. The dimension of the component are presented in a schematic figure in Fig. 10a. As in Selamet et al.[13], the diameter of the duct is $d_p = 4.859$ cm. The optimization variables are as follows. The diameter of the resonator chamber x_1 can vary between $[1, 15]$ cm, the diameter of connecting pipe x_2 can vary between $[1, 4]$ cm, the length of the connecting duct x_3 can vary between $[0.1, 8.5]$ cm and the length of the resonator chamber x_4 can vary between $[1, 15]$ cm. Transmission loss is optimized in two frequency ranges: between 80-100 Hz and 160-180 Hz, and the frequency sets (see Eq. (9)) are set to $\boldsymbol{\omega} = [160, 170, 180]$ Hz and $\boldsymbol{\iota} = [70, 80, 90]$ Hz. As in previous test problem, the population size is set to $n_{pop} = 100$.

In Fig. 11, there are four non-dominated fronts of objective functions in Eq. (9) that are obtained by NSGA-II after 30 generations. Also here it is seen that fronts are converged to the same line. Before optimization, the average values of the fitness function values of randomly generated initial population were $f_1 = -3.3$ dB and $f_2 = -1.4$ dB.

In Fig. 12, the transmission loss as a function of frequency is plotted for selected optimal solutions. The example solutions for these points are also plotted in Fig. 10b. It is seen in Fig. 12 that in this case, that within the chosen frequency range, it is not possible to obtain significant transmission loss at both frequency ranges simultaneously, as only one peak in transmission loss curve occur. A good solution, however, is obtained for both frequency ranges separately.

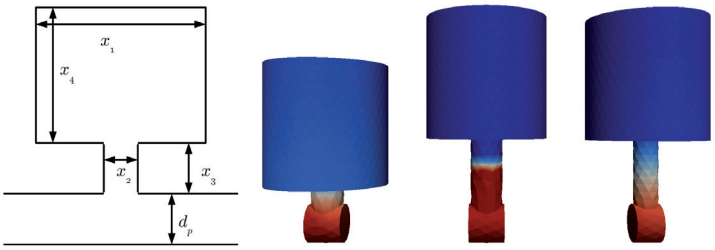

(a) (b)

Figure 10: On the left figure, there is a diagram of a Helmholtz resonator component used in test case #4. On the right figure, the pressure time average of selected optimal solutions is plotted for test problem #4. The figures are plotted at 170, 170 and 90 Hz, correspondingly.

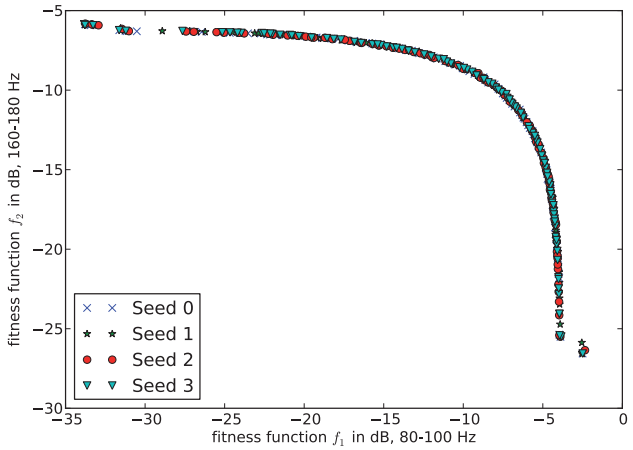

Figure 11: The non-dominated fronts for test case #4 are plotted, four different random seeds.

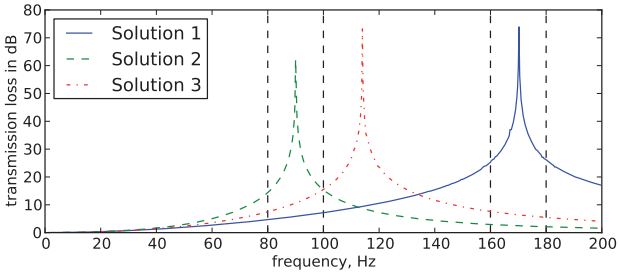

Figure 12: The transmission loss as a function of frequency. Transmission loss is maximized at frequency ranges 80-100 Hz and 160-180 Hz. The solution 1 has been chosen at point $f_1 = -33.8$ dB, $f_2 = -5.9$ dB, solution 2 at $f_1 = -6.5$ dB, $f_2 = -11.2$ dB and solution 3 at $f_1 = -2.5$, $f_2 = -26.6$ dB.

5 Conclusions

Multiobjective shape optimization in a muffler with respect to sound transmission loss has been considered. The shape of the muffler component in a duct system is optimized. NSGA-II has been used as an multiobjective optimization method and acoustics has been simulated by finite element method. A hybrid method has been considered to match the acoustical solution of the muffler with analytical multimodal solution in inlet and outlet ducts.

Two frequency ranges were optimized simultaneously. For each test problem, example solutions were chosen from the non-dominated front that was given by NSGA-II optimizer algorithm. The transmission loss as a function of frequency was plotted for them and the time average of pressure was plotted to a single frequency. A good sound transmission loss, from 30 dB to 50 dB, was obtained at chosen frequencies in each test problem. The optimization significantly improved the objective functions when compared to the initial random designs.

The robustness of the method was tested by considering test problems with four different random number generator seed numbers. It was found that similar results were found for all tested seed numbers, which implicates that the method converges to a near-optimal solution and that the solution does not depend on initial solutions with considered test problems.

Because of the mode matching that was considered on inlet and outlet boundaries, the hybrid method provides accurate and realistic modeling of acoustics in muffler component. The method can be used with any frequency that the computation time and memory allows. Finite element method allows almost arbitrary three-dimensional shape of the design and boundary conditions, which brings versatile possibilities to the formulation of muffler component optimization. Combined with the NSGA-II optimization algorithm, the method offers generic, robust and advanced approach to many three-dimensional muffler optimization problems.

Acknowledgment

Authors want to thank Jari Toivanen for valuable co-operation and comments during the manuscript preparation.

References

[1] J. M. Egana, J. Diaz, J. Vinolas, Active control of low-frequency broadband air-conditioning duct noise, Noise Control Eng. 51 (5) (2003) 292–299.

[2] H. J. Lee, Y. C. Park, C. Lee, D. H. Youn, Fast active noise control algorithm for car exhaust noise control, Electron. Lett. 36 (14) (2000) 1250–1251.

[3] M. L. Munjal, Acoustics of ducts and mufflers, Chichester: John Wiley, 1987.

[4] L.-J. Yeh, Y.-C. Chang, M.-C. Chiu, Shape optimal design on double-chamber mufflers using simulated annealing and a genetic algorithm, Turkish J. Eng. Env. Sci. 29 (2005) 207–224.

[5] T. Airaksinen, A. Pennanen, J. Toivanen, A damping preconditioner for time-harmonic wave equations in fluid and elastic material, J. Comput. Phys. 228 (5) (2009) 1466–1479.

[6] R. Kirby, Modeling sound propagation in acoustic waveguides using a hybrid numerical method, J. Acoust. Soc. Am. 124 (4) (2008) 1930–1940.

[7] R. J. Astley, Fe mode-matching schemes for the exterior helmholtz problem and their relationship to the fe-dtn approach, Commun. Numer. Meth. En. 12 (4) (1996) 257–267.

[8] J. Haslinger, R. A. E. Mäkinen, Introduction to Shape Optimization: Theory, Approximation, and Computation, Society for Industrial and Applied Mathematics, Philadelphia, PA, USA, 2003.

[9] R. A. E. Mäkinen, J. Periaux, J. Toivanen, Multidisciplinary shape optimization in aerodynamics and electromagnetics using genetic algorithms, Int. J. Numer. Meth. Fl. 30 (2) (1999) 149–159.

[10] K. Deb, A. Pratap, S. Agarwal, T. Meyarivan, A Fast Elitist Multi-Objective Genetic Algorithm: NSGA-II, IEEE T. Evolut. Comput. 6 (2000) 182–197.

[11] R. Kirby, J. Lawrie, A point collocation approach to modelling large dissipative silencers, J. Sound Vib. 286 (1-2) (2005) 313–339.

[12] R. Barbieri, N. Barbieri, Finite element acoustic simulation based shape optimization of a muffler, Appl. Acoust. 67 (4) (2006) 346–357.

[13] A. Selamet, P. Radavich, N. Dickey, J. Novak, Circular concentric Helmholtz resonators, J. Acoust. Soc. Am. 101 (1) (1997) 41–51.

[14] R. B. Agrawal, K. Deb, Simulated binary crossover for continuous search space, Complex Syst. 9 (1995) 115–148.

[15] J. Schöberl, NETGEN - an advancing front 2D/3D-mesh generator based on abstract rules, Comput. Visual. Sci 1 (1997) 41–52.

[16] Numerola Ltd, P.O.Box 126 Väinönkatu 7 C, 40101 Jyväskylä, `http://www.numerola.fi`.

[17] F. Ihlenburg, Finite element analysis of acoustic scattering, Vol. 132 of Applied Mathematical Sciences, Springer-Verlag, New York, 1998.